Effect of Idealized Asymmetric Inhibitor Stubs on Circumferential Flow in the Space Shuttle SRM

Alok K. Majumdar,* R. Harold Whitesides,† and Susan L. Jenkins‡
SRS Technologies, Huntsville, Alabama
and
David L. Bacchus§
NASA Marshall Space Flight Center, Huntsville, Alabama

Computational fluid dynamic analyses have been performed to calculate circumferential pressure and velocity gradients in the vicinity of an asymmetric inhibitor stub in the port of the Space Shuttle solid rocket motor. The three-dimensional Navier-Stokes equations were solved by an iterative finite volume algorithm, SIMPLE, incorporated in a general purpose computer code, FLUENT. Turbulence was represented by way of effective viscosity, which was calculated from local turbulence energy and its dissipation rate (K-ϵ model). The numerical predictions were compared with the measurements from a 7.5% scale, cold-flow model of the redesigned solid rocket motor. The calculated circumferential pressure distribution upstream of the inhibitor stub compares well with the measured data.

Introduction

THE purpose of this investigation was to determine the nature of the three-dimensional port flowfield in the vicinity of the aft field joint of the Space Shuttle redesigned solid rocket motor (RSRM). Specific objectives included the quantification of the circumferential pressure and velocity gradients in the motor port in the immediate vicinity of asymmetric inhibitor stubs at the aft field joint. Nonuniform erosion of the rubber inhibitor, which protrudes from the wall into the port flowfield, gives rise to circumferential flow gradients which increase the heat load on the joint and adjacent insulation materials. Separate studies of the detailed flow and heating in the crevices of the joint required, as boundary conditions, a knowledge of the potential circumferential pressure distribution in the port of the motor which could drive flow into the joint crevices on one side of the motor and circumferentially around the joint to exit on the opposite side. Therefore, a major objective of this study[1] was to determine the circumferential pressure gradients for a range of hypothetical asymmetric inhibitor geometries.

The basic approach included the use of computational fluid dynamics (CFD)[2-5] and experimental cold flow testing of subscale models.[6] A 7.5%-scale model of the RSRM was tested with various nonuniform inhibitor geometries, and circumferential flow patterns were mapped with wall oil-flow techniques. Circumferential pressure gradients were measured in the vicinity of the simulated field joint. This testing was done with unheated air in the NASA Marshall Space Flight Center's airflow facility. The data from this experimental program were used to validate the CFD methodology by comparing the data with CFD predictions for the experimental geometry and flow conditions. The designs for the experimental inhibitor configurations were hypothetical and idealized for simplicity to expedite the test program. In the actual RSRM, the rubber inhibitors would bend over in the downstream direction rather than protrude perpendicularly into the stream as represented

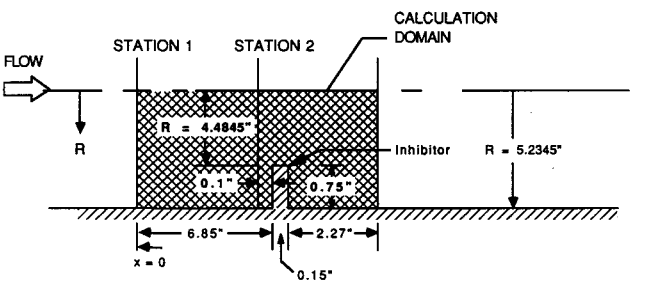

Fig. 1a Schematic sketch of the subscale model showing the calculation domain.

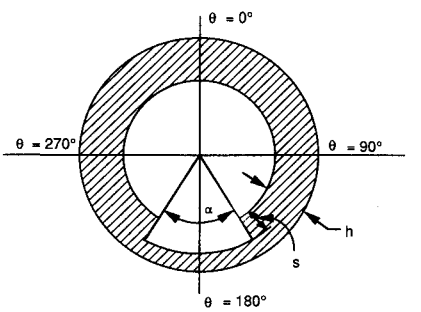

Fig. 1b Schematic sketch of slotted inhibitor configuration.

Received July 5, 1988; presented as Paper 88-3319 at the AIAA/ASME/SAE/ASEE 24th Joint Propulsion Conference, Boston, MA, July 11-13, 1988; revision received July 12, 1989.

*Senior Staff Scientist.
†Senior Staff Scientist. Associate Fellow AIAA.
‡Senior Engineer.
§Team Leader, Induced Environment Branch.

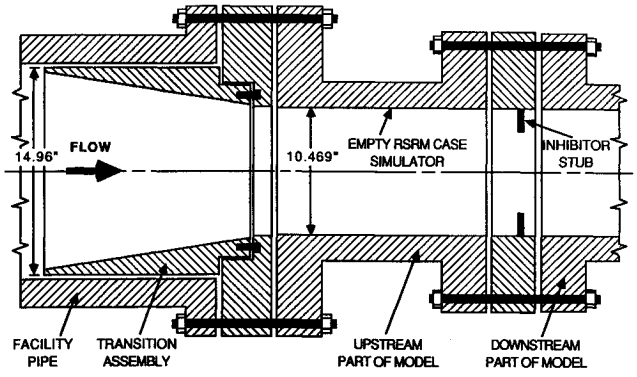

Fig. 2 The interface between Marshall Space Flight Center airflow facility and subscale model.

Table 1 Inhibitor configurations analyzed

Inhibitor height, h (in.)	Slot angle, α (deg)	Slot depth, s (in.)
0.75	180	0.75
0.75	180	0.50
0.75	180	0.25
0.75	90	0.75
0.75	30	0.75
0.75	12	0.75
0.75	12	0.50
0.75	12	0.25
0.75	Offset[a]	Offset[a]
0.45	90	0.45

[a]Offset center of hole in circular orifice plate by 0.125 in. such that max inhibitor height occurs at $\theta = 180$ deg and min inhibitor height occurs at $\theta = 0$ deg.

by the test configurations. Also there would be wall mass addition from the burning propellant adjacent to the joint which was not modeled in the experiment. Therefore, the experimental results are not directly representative of the actual conditions in the RSRM. However, the test results did serve to validate the basic CFD methodology. In separate analyses[7,8] not reported here, the CFD models were modified to include the effects of curved inhibitor stubs, wall mass addition, and changes in propellant geometry and port-flow conditions to represent various RSRM burn times.

Flow Configuration

A schematic sketch of the subscale model with eroded inhibitor is shown in Figs. 1a and 1b. In the inhibitor configuration shown, in Fig. 1b, part of the inhibitor is eroded. Inlet velocity profiles are measured at station 1. Circumferential pressure distributions are measured at station 2, which is immediately upstream of the inhibitor. Circumferential pressure distribution is caused by a variation in the inhibitor height around the circumference. The static pressure is higher at $\theta = 0$ deg than at $\theta = 180$ deg, which generates a circumferential flow. A three-dimensional flow analysis is therefore needed to predict circumferential flow in this configuration.

CFD Methodology

A general purpose computer code, FLUENT,[5] was used to solve the three-dimensional Navier-Stokes equation in conjunction with the conservation equation for turbulence energy and dissipation rate. This code uses the semi-implicit method for pressure linked equations (SIMPLE) algorithm of Patankar and Spalding,[2] a thorough description of which is given in the book by Patankar.[3] Turbulence is represented by way of effective viscosity expressed as a function of local

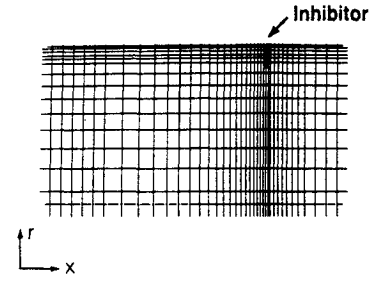

Fig. 3 Finite-difference grid in radial-axial plane (0.75 in.-high inhibitor, 180-deg slot angle, and 0.75-in. slot depth).

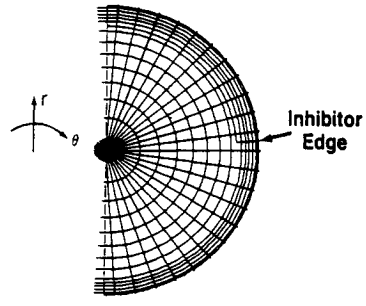

Fig. 4 Finite-difference grid in radial-circumferential plane (0.75 in.-high inhibitor, 180-deg slot angle, and 0.75-in. slot depth).

turbulence energy K and its dissipation rate ϵ[4]. The momentum transport processes near the wall have been modeled through wall functions. The use of wall functions with complex three-dimensional recirculating flow is subject to question; however, the primary objective of this study was the determination of the circumferential pressure distribution, which is primarily driven by inviscid effects of the asymmetric inhibitor protruding into the approaching port flowfield. Thus, any inaccuracies associated with resolving the velocity gradient at the wall with wall functions in the three-dimensional recirculating flowfield are not an issue for this study.

The conservation equations for mass and momentum in the axial u, radial v, and circumferential w direction, turbulence energy K and dissipation rate ϵ solved by the code can be expressed in the following general form.

Mass:

$$\text{div}\ (\rho \overline{V}) = 0 \tag{1}$$

Momentum and scalar properties:

$$\text{div}\ (\rho \overline{V}\phi - \Gamma_\phi \text{grad}\phi) = S_\phi \tag{2}$$

where ϕ is general conserved property which stands for u, v, w, K, and ϵ; Γ_ϕ is exchange coefficient for ϕ; and S_ϕ is source of ϕ per unit volume. A set of algebraic equations are obtained by integrating Eqs. (1) and (2) over finite volumes that are used to discretize the calculation domain (Fig. 1a). This set of simultaneous algebraic equations is solved by an iterative scheme which starts from arbitrary initial conditions and converges to the correct solution after performing a number of iterations.

Experimental Setup

The cold-flow test setup is a 7.5%-scale model of the aft section of the RSRM from the aft case field joint to the nozzle throat.[6] An assembly sketch of the model is shown in Fig. 2. A transition assembly was used as an interface between the

16-in. facility pipe and the 10.469-in. internal diameter. The nozzle throat diameters is 4.040 in., and the chamber has a diameter of 10.469 in., which represents the diameter of the insulation surface. The nitrile butadiene rubber (NBR) inhibitor stub geometries are simulated with steel "orifice" plate inserts (see Fig. 1b) incorporating notches of various depths and angles. The radial heights of the inhibitor stub simulators were scaled from post-test inspection of flight solid rocket motors. The tests were conducted at a reference pressure of 350 psia. Calculated Mach number, average velocity, and flow rate are 0.0866, 98.60 ft/s, and 102.59 lbm/s, respectively. Differential pressure transducers with operating ranges of 0–10 psi and 0–15 psi and absolute pressure transducers with an operating range of 0–500 psia were utilized for pressure measurements. The purpose of using differential pressure transducers was to be able to measure accurately the small circumferential pressure differentials.

Results and Discussion

The geometrical parameters defined in Fig. 1b for 10 test configurations are listed in Table 1. Predicted circumferential pressure distributions immediately upstream of the inhibitor were compared with the measurements. Computer-generated graphics were used to describe the finite-difference grid distribution and the three-dimensional flowfield near the inhibitor.

A 40 (axial direction) × 15 (radial direction) × 25 (circumferential direction) grid distribution of 15,000 nodes was chosen to perform all the calculations presented in this paper. The finite difference grid in the radial-axial plane is shown in Fig. 3; the cross-sectional plane is shown in Fig. 4. A sensitivity anlysis of the grid distribution on the circumferential pressure difference was performed. The result of the sensitivity analysis showed that, with the addition of 1500 grid nodes in the vicinity of the edge of the inhibitor, the circumferential pressure differential between $\theta = 0$ and 180 deg in the near-wall node changed only by 3%. It may be mentioned here that a nonuniform grid distribution in the circumferential direction was employed for the lower slot angles. This was done in order to locate more grids in the region of steep pressure gradient.

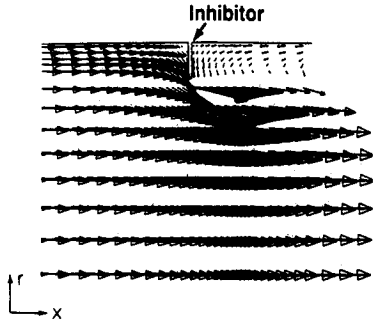

Fig. 5 Velocity vector in radial-axial plane (0.75-in.-high inhibitor, 180-deg slot angle, and 0.75-in. slot depth).

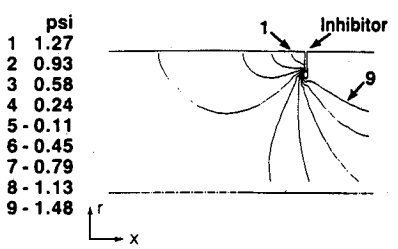

Fig. 6 Relative pressure distribution ($P - P_{inlet}$) in radial-axial plane (0.75-in. inhibitor, 180-deg slot angle, and 0.75-in. slot depth).

The numerical solution was regarded converged when the normalized integrated imbalance of all conserved variables (i.e., mass, u, v, w, K, and ϵ) in the calculation domain was less than 0.1%. It took approximately 350 iterations to obtain a converged solution from an arbitrary initial guess. Fewer number of iterations, however, were needed when the initial guess was the converged solution of a case not largely different from the case being considered. The built-in convergence criterion in FLUENT was based on checking conservation error and not on percentage variation of variables in successive iterations. A converged solution was then restarted, and 200 more iterations were performed. The change in circumferential pressure difference over 180 deg was found to be only 0.25%.

The calculated flowfield for the 0.75-in.-high inhibitor, 180-deg slot angle, and 0.75-in. slot depth is shown in Figs. 5–8. The velocity field in the axial plane at $\theta = 0$ deg is shown in Fig. 5, and this figure shows a strong recirculation in the downstream portion of the inhibitor. The pressure distribution (Fig. 6) supports this observation. It also shows a region of high-pressure gradient near the top edge of the inhibitor. The pressure distribution in the radial circumferential plane immediately upstream of the inhibitor is shown in Fig. 7. A strong circumferential gradient of pressure is observed near the slot edge, and a strong radial gradient is observed near the inhibitor edge. The circumferential velocity distribution in the radial circumferential plane is shown in Fig. 8. The largest circumferential velocity is found to occur near the slot edge.

The calculations were performed for three 180-deg slot angle inhibitors having slot depths of 0.75, 0.50, and 0.25 in., respectively. The comparison between the predicted and the measured circumferential pressure distribution 0.1 in. upstream of the inhibitor appears in Figs. 9–11. There is good agreement between theory and data on the general shape and trend of the circumferential pressure gradient. The observed discrepancy in the maximum value of the circumferential pressure difference is possibly due to difficulties in resolving, both

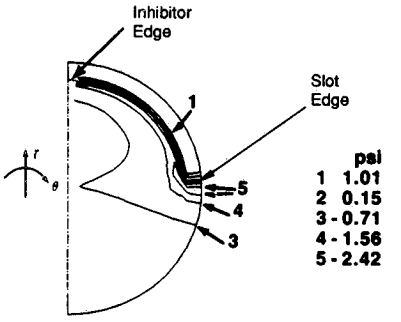

Fig. 7 Relative pressure distribution ($P - P_{inlet}$) in radial-circumferential plane (0.75-in.-high inhibitor, 180-deg slot angle, and 0.75-in. slot depth).

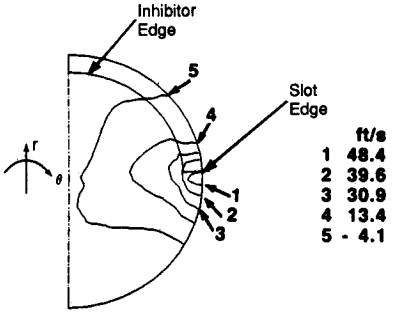

Fig. 8 Circumferential velocity distribution in radial-circumferential plane (0.75-in.-high inhibitor, 180-deg slot angle, and 0.75-in. slot depth).

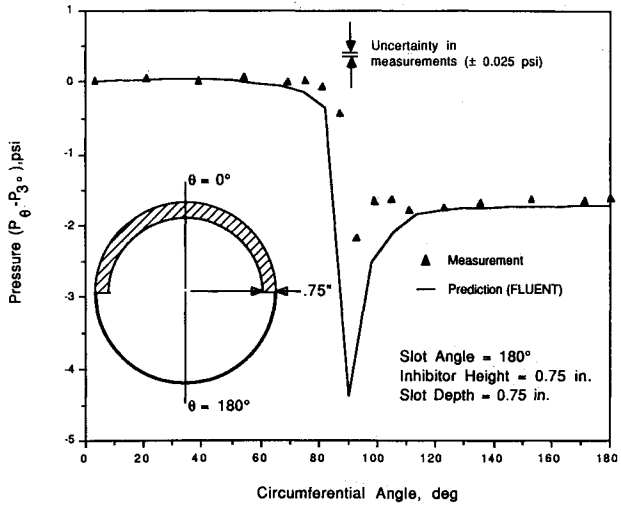

Fig. 9 Predicted and measured circumferential pressure distribution immediately upstream of inhibitor (h = 0.75 in., α = 180 deg, s = 0.75 in.).

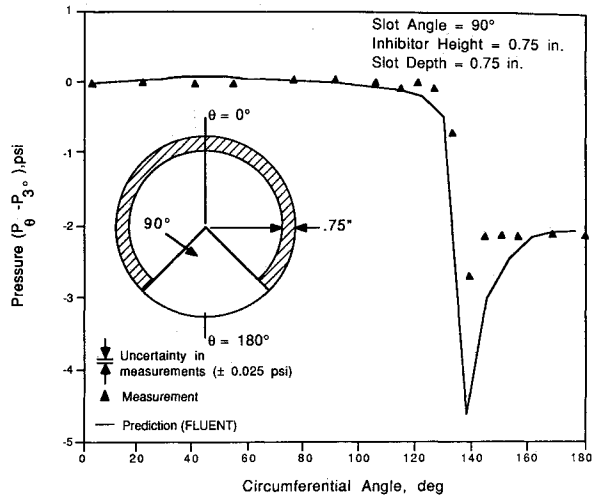

Fig. 12 Predicted and measured circumferential pressure distribution immediately upstream of inhibitor (h = 0.75 in., α = 90 deg, s = 0.75 in.).

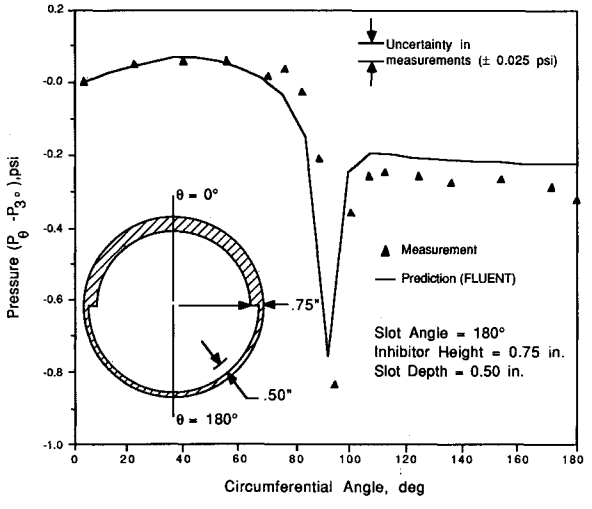

Fig. 10 Predicted and measured circumferential pressure distribution immediately upstream of inhibitor (h = 0.75 in., α = 180 deg, s = 0.50 in.).

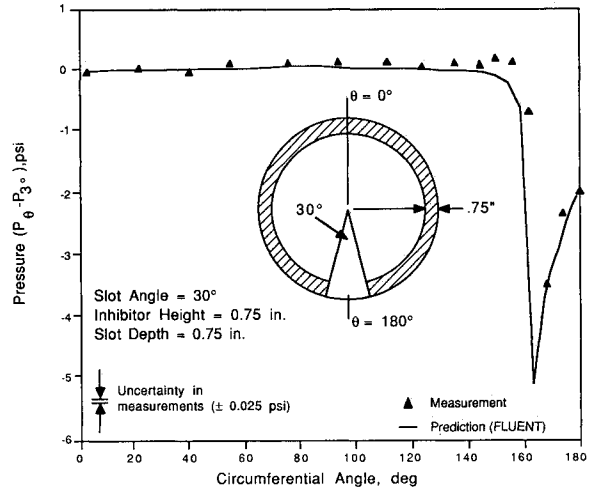

Fig. 13 Predicted and measured circumferential pressure distribution immediately upstream of inhibitor (h = 0.75 in., α = 30 deg, s = 0.75 in.).

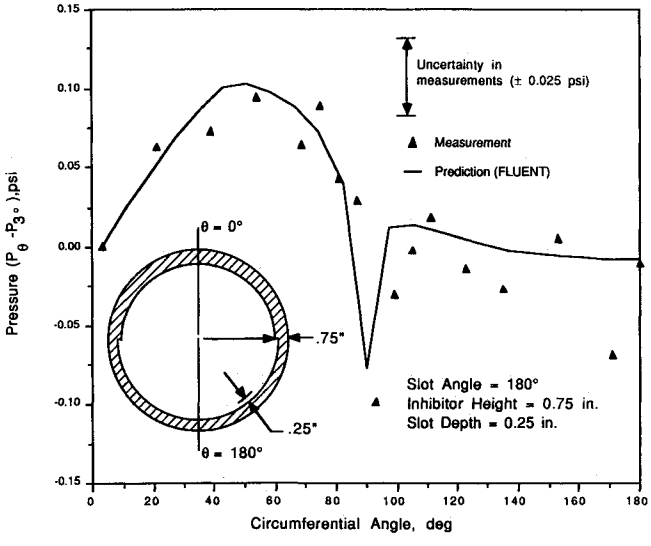

Fig. 11 Predicted and measured circumferential pressure distribution immediately upstream of inhibitor (h = 0.75 in., α = 180 deg, s = 0.25 in.).

experimentally and analytically, the steep pressure gradient near the slot edge. The measurements may not have picked up the minimum pressure with the existing instrumentation and/or the prediction may be off at the minimum point due to the extremely steep pressure gradient.

Figures 9–11 show a trend with slot depth. When the slot depth was equal to the stub height (see Fig. 9), the circumferential pressure distribution did not change until the neighborhood of the slot edge was reached. When the slot depth was less than the stub height, the circumferential pressure increased initially with azimuth angle then decreased as before when the slot edge was reached. When a shallower slot was used, the effect was more pronounced. This effect was due to an asymmetric inlet velocity profile at station 1 (see Fig. 1a). With lower slot depths, the circumferential pressure difference was relatively small, and therefore effects of asymmetry in the measured velocity profile[6] were reflected more clearly in the smaller scale plots of circumferential distribution of relative pressure.

The comparison between predicted and measured circumferential pressure distribution for full depth slots with slot angles of 90 and 30 deg are shown in Figs. 12 and 13, respectively. The comparisons appear satisfactory except very near the slot

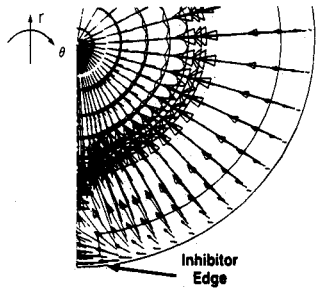

Fig. 14 Magnified view of velocity field near the slot edge (0.75-in. inhibitor, 12-deg slot angle, and 0.50-in. slot depth).

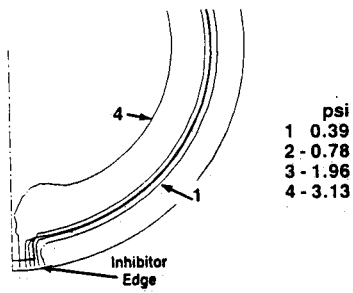

Fig. 15 Magnified view of pressure distribution near the slot edge (0.75-in. inhibitor, 12-deg slot angle, and 0.50-in. slot depth).

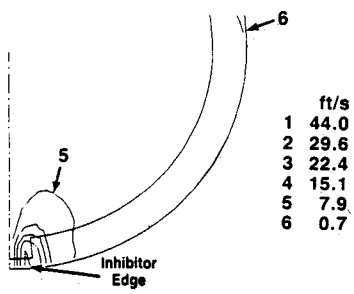

Fig. 16 Magnified view of circumferential velocity distribution near the slot edge (0.75-in.-high inhibitor, 12-deg slot angle, and 0.50-in. slot depth).

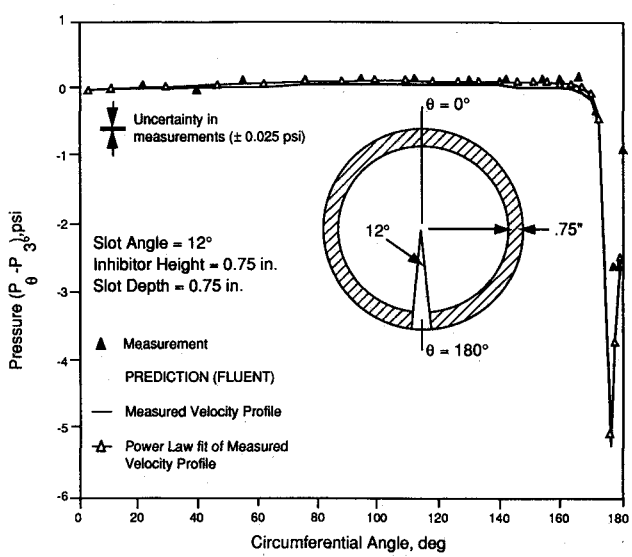

Fig. 17 Predicted and measured circumferential pressure distribution immediately upstream of inhibitor (h = 0.75 in., α = 12 deg, s = 0.75 in.).

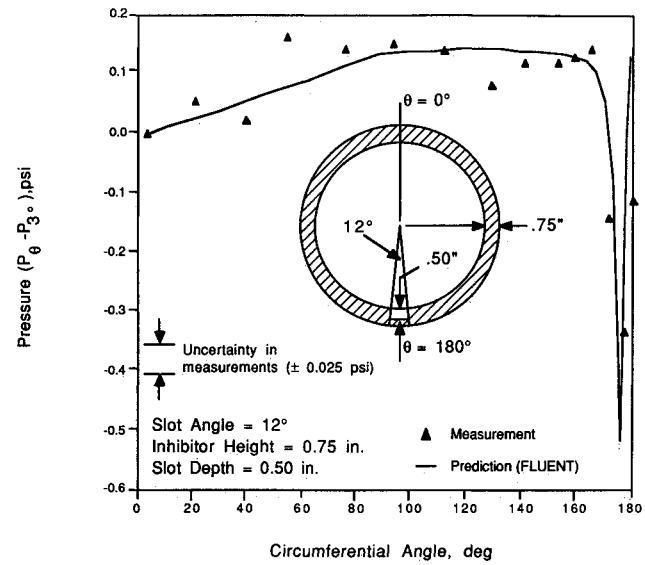

Fig. 18 Predicted and measured circumferential pressure distribution immediately upstream of inhibitor (h = 0.75 in., α = 12 deg, s = 0.25 in.).

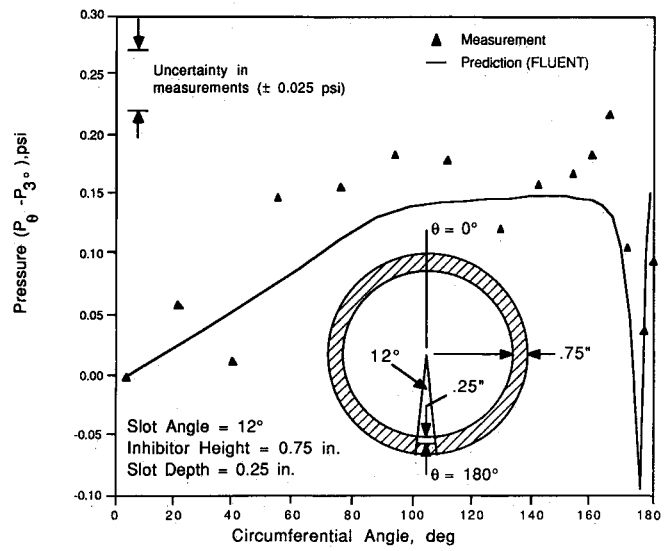

Fig. 19 Predicted and measured circumferential pressure distribution immediately upstream of inhibitor (h = 0.75 in., α = 12 deg, s = 0.25 in.).

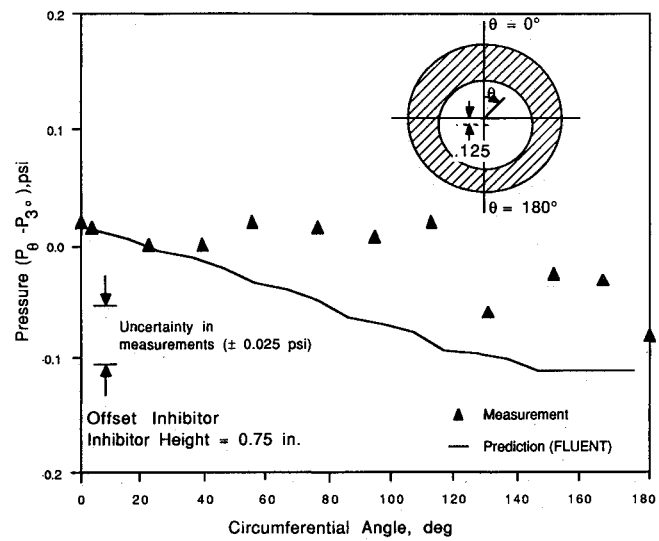

Fig. 20 Predicted and measured circumferential pressure distribution immediately upstream of offset inhibitor.

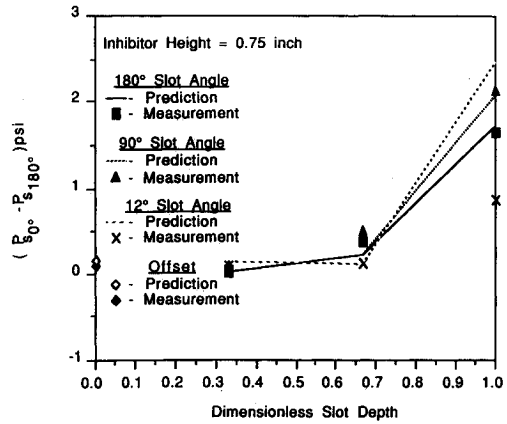

Fig. 21 Predicted and measured circumferential pressure differences for different slot configurations.

edge. Analysis predicted a stronger gradient than that observed in the experiment.

Magnified views of the velocity field, pressure, and circumferential velocity distribution for the 12-deg slot angle appear in Figs. 14–16, respectively. Strong radial and circumferential velocity components were observed near the slot edge. Comparisons between measurements and predictions appear in Figs. 17–19 for slot depths of 0.75, 0.50, and 0.25 in., respectively. Figure 17 shows the comparison between two predicted circumferential pressure distributions. In one case, the measured velocity profile has been used at the inlet plane and in the other case, a power law fit of the measured velocity profile has been used. No significant difference was observed between the two predictions.

This series of tests were designed to determine the effect of various unsymmetrical inhibitor configurations on the flow characteristics at the aft case field joint. One of the configurations was called the "offset" inhibitor. The assumption was made that the inhibitor was eroded in an asymmetric but continuous manner. There was a larger erosion at $\theta = 180$ deg than at $\theta = 0$ deg; however, the rate of erosion was continuous between $\theta = 0$ and 180 deg. The offset was 0.125 in. such that the maximum inhibitor height of 0.875 in. occurred at 0 deg, and the minimum inhibitor height of 0.625 in. occurred at 180 deg.

A comparison between predicted and measured circumferential pressure distribution immediately upstream of the offset inhibitor is shown in Fig. 20.

A summary comparison of the predicted and measured circumferential pressure differences between 0 and 180 deg for various slot configurations appears in Fig. 21. Circumferential pressure difference is plotted vs the dimensionless slot depth. The dimensionless slot depth was defined as the ratio of slot depth to inhibitor height.

Conclusions

Circumferential pressure drop for the slotted inhibitors is a strong function of slot depth and relatively weak function of slot angle. The height of the inhibitor is also an important parameter affecting circumferential pressure drop. Comparisons with measured data are satisfactory—particulalry for higher slot angles and higher slot depths.

The observed discrepancy between measurements and predictions can be mainly attributed to 1) for a low slot angle, the pressure gradient is very steep near $\theta = 180$ deg; 2) for low slot depth, pressure differences are very small and are close to the accuracy level of pressure gauges used in the measurement. The overall comparison between measurements and predictions provided a validation of the CFD methodology used in this study. Therefore the results of this program were successful in supporting the credibility of the CFD analyses performed for the full scale RSRM to determine circumferential pressure gradients in the vicinity of the field joints using real motor geometry and flow boundary conditions.

Acknowledgments

This work was performed for the NASA Marshall Space Flight Center through a Morton Thiokol, Inc. contract. The authors wish to acknowledge the support of the NASA/Marshall Space Flight Center Air Flow Facility testing and instrumentation personnel. Other significant contributing SRS personnel include Ashok Ghosh and Joe Cody.

References

[1]"Circumferential Flow Field Analyses for the Subscale Model of the SRM Aft Field Joint," SRS Technologies, Huntsville, AL, Rept. SRS/STD-TR88-12; also NASA Marshall Space Flight Center Rept. 1523, Feb. 1988.

[2]Patankar, S. V. and Spalding D. B., "A Calculation Procedure for Heat, Mass and Momentum Transfer in Three Dimensional Parabolic Flows," *International Journal of Heat Mass Transfer,* Vol. 15, 1972, pp. 1787–1806.

[3]Patankar, S. V., *Numerical Heat Transfer and Fluid Flow,* Hemisphere, Washington, DC.

[4]Launder, B. E. and Spalding, D. B., "The Numerical Computation of Turbulent Flows," *Computer Methods in Applied Mechanics and Engineering,* Vol. 3, 1974, pp. 269–289.

[5]FLUENT MANUAL, Version 2.9, Creare Incorporated, Hanover, NH, Rept. TN-369, Feb. 1987.

[6]"Subscale Cold Flow Tests (Aft Field Joint), MSFC Test 21, Phase II," SRS Technologies, Huntsville, AL, Rept. SRS/STD-TR88-13; also NASA Marshall Space Flight Center, Rept. 1512, Nov. 1987.

[7]"SRM Port Flowfield Analysis at The Field Joints," SRS Technologies, Huntsville, AL, Technical Rept. SRS/STD-TR87-61; also NASA Marshall Space Flight Center Rept. 1515, July 1987.

[8]"Circumferential Flow Field Analysis at the Aft Field Joint Due to Propellant Slump and Non-Uniform Erosion of Inhibitor," SRS Technologies, Huntsville, AL, Technical Rept. SRS/STD-TR88-07; also NASA Marshall Space Flight Center Rept. 1516, Oct. 1987.